Theoretical characterization of the spectral density of the water-soluble chlorophyll-binding protein from combined quantum mechanics/molecular mechanics molecular dynamics simulations

Andreana M. Rosnik[ab] and Carles Curutchet[a*]

[a]Department de Fisicoquímica, Facultat de Farmàcia, Universitat de Barcelona, Av. Joan XXIII s/n, Barcelona 08028, Spain

[b]Department of Chemistry, University of California, Berkeley, CA, 94720, USA

Abstract

Over the past decade, both experimentalists and theorists have worked to develop methods to describe pigment-protein coupling in photosynthetic light-harvesting complexes in order to understand the molecular basis of quantum coherence effects observed in photosynthesis. Here we present an improved strategy based on the combination of quantum mechanics/molecular mechanics (QM/MM) molecular dynamics (MD) simulations and excited state calculations to predict the spectral density of electronic-vibrational coupling. We study the water-soluble chlorophyll-binding protein (WSCP) reconstituted with *Chl a* or *Chl b* pigments as the system of interest and compare our work with data obtained by Pieper and co-workers from differential fluorescence line-narrowing spectra (Pieper et al. J. Phys. Chem. B 2011, 115 (14), 4042-4052). Our results demonstrate that the use of QM/MM MD simulations where the nuclear positions are still propagated at the classical level leads to a striking improvement of the predicted spectral densities in the middle and high frequency regions, where they nearly reach quantitative accuracy. This demonstrates that the so-called "geometry mismatch" problem related to the use of low-quality structures in QM calculations, not the quantum features of pigments high-frequency motions, causes the failure of previous studies relying on similar protocols. Thus, this work paves the way toward quantitative predictions of pigment-protein coupling and the comprehension of quantum coherence effects in photosynthesis.

1. Introduction

Photosynthesis is the process by which sunlight is captured and converted into chemical energy, ultimately sustaining the life of essentially all organisms on earth. Despite its importance to life, the actual mechanism by which photons are captured and their energy is passed among pigment-protein complexes toward reaction centers is still heavily debated. In particular, the recent discovery that electronic energy transfer (EET) in photosynthesis involves quantum coherence, or correlation between quantum states in multiple objects, has challenged the traditionally assumed Förster incoherent hopping mechanism.[1–3] Understanding the molecular basis sustaining quantum coherence could lead to the design of more robust, affordable means to obtain renewable energy, *e.g.,* a new generation of solar cells.[4] Even if the impact of quantum coherence on light harvesting efficiency is still controversial,[3] such knowledge could also be useful for designing quantum computing technologies, where a long-standing goal is to maintain coherences among qubits at room temperature.[5]

Researchers previously considered that quantum coherence could not be involved in photosynthetic light harvesting due to the thermal disorder present in biological systems. However, when coherences were observed to survive for hundreds of femtoseconds,[6–8] it became evident that the protein environment and its structural dynamics play a critical role in the light harvesting process.[2,9,10] In particular, quantum coherence seems to be intimately related to the *structured* nature of the protein environment, as opposed to the behavior of a random thermal noise that should favor decoherence. One hypothesis supposes that correlated fluctuations in the individual pigments electronic energy levels, or site energies, could give rise to long-lived coherences.[7] Nonetheless, theoretical studies combining quantum chemistry and classical molecular dynamics (MD) simulations predict such correlations to be negligible.[11,12] Another popular hypothesis emphasizes the coupling of protein vibrations to pigments excitations, which could support coherence in cases where the vibrational energy commensurates the energy gap among exciton states.[13,14]

The emerging consensus suggests that EET in photosynthesis often occurs in an intermediate coupling regime. This implies that neither pigment-pigment nor pigment-protein interactions can be treated perturbatively when solving the dynamics of EET, as is done in the popular Förster or Redfield theories, because the magnitudes of these interaction strengths are similar. Much progress has been made to develop theoretical models simulating EET dynamics in the intermediate regime.[3] That said, the outcome of these models critically depends on the tools used to parameterize the photosynthetic system at hand – namely, the site energies, the electronic couplings, and the spectral density of exciton-phonon coupling that quantifies the pigment-protein interactions. Whereas recent research has made substantial progress towards accurately determining model Hamiltonian parameters (site energies and couplings) both from theory and from experiment,[15–17] the determination of the spectral density of individual pigments in a pigment-protein complex – the quantity needed to understand the molecular basis of quantum coherence – still presents a great challenge to the field, primarily since a large number of protein vibrations couple to many pigment electronic transitions over multiple timescales. Consequently, it is quite difficult to construct experiments in which the correlation between pigments electronic excited states and protein vibrational states can be discerned. Site-selective spectroscopies provide an appealing means to determine spectral densities; however, these techniques often only probe the lowest-energy fluorescing pigments in the complex.[18]

An intriguing alternative to experiment is the theoretical determination of spectral densities. Several groups have contributed important advances in this direction.[19–34] The typical technique involves the extraction of the spectral density from the Fourier transform of the autocorrelation function of site energy fluctuations, the latter estimated using mixed quantum mechanical/molecular mechanical (QM/MM) calculations performed along a classical MD trajectory.[19,22,24] This strategy has been applied to several pigment-protein complexes by performing semi-empirical Zerner's intermediate neglect of differential overlap (ZINDO) or time-dependent density functional theory (TD-DFT) calculations in the presence of the protein atomic charges, which mimic the electrostatic influence of the protein on the pigments' excited states. Recently, we have explicitly accounted for protein polarization effects on the pigment-protein coupling using a polarizable force field.[31] Nevertheless, the spectral densities predicted in this way systematically show strongly overestimated peaks in the high frequency region of the spectrum, a problem often ascribed to the classical nature of the MD simulations performed,

which prevents the capture of the quantum mechanical features of such high-frequency modes. Another limitation of this strategy arises from the "geometry-mismatch" problem, as low-quality geometries extracted from the classical simulation are used for QM excited state calculations.

In this publication, we present an improved strategy based on the combination of semi-empirical QM/MM MD simulations[35] with polarizable QM/MMpol calculation of the excited state properties.[36,37] We apply this novel approach to the prediction of spectral densities of *Chl a* and *Chl b* in class IIb water-soluble chlorophyll-binding protein (WSCP). Our results are critically compared with predictions from classical MD simulations as well as from detailed differential fluorescence line-narrowing data.[38–40] They reveal that when the MD trajectory is obtained along a QM/MM potential energy surface, theoretical predictions can capture the intramolecular features characterizing the spectral densities of the chlorophylls in WSCP to a surprisingly high degree of accuracy.

The term “WSCP” actually implies two different classes of proteins, of which there are multiple types. The WSCP complex studied here corresponds to class IIb WSCP from *Lepidium virginicum* (Virginia pepperweed), whose crystal structure was solved by Horigome *et al*.[41] This structure is organized as a homotetramer, where each monomer binds one *Chl a* or *Chl b* molecule, as illustrated in Figure 1. This leads to a dimer-of-dimers organization of the chlorophylls. WSCP is not a photosynthetic protein but rather a chlorophyll carrier protein found in higher plants; its proposed function is to scavenge for and hoard chlorophyll when the plant experiences stress.[41] The tractable size, dimer-of-dimer symmetry, presence of multiple pigments, and proximity of the chlorophylls within a dimer greatly simplify complexities that are observed in photosynthetic complexes, making WSCP a simple yet effective model to investigate in detail the role of pigment-pigment and pigment-protein interactions in photosynthetic systems. Most theoretical and spectroscopic studies, including steady-state spectra, transient absorption, difference fluorescence line-narrowing, and hole-burning experiments, have so far addressed the properties of class IIa WSCP,[38,39,42–45] which binds up to two chlorophylls per complex. Only recently, 2D electronic spectroscopy experiments have also been presented for class IIb WSCP.[46] Some studies have shown that the crystal structure of class IIb WSCP can be used to describe the optical properties of class IIa WSCP, suggesting a similar Chl binding motif in both cases.[47,48] Following this idea, we adopt the class IIb crystal structure of WSCP to simulate the spectral

density determined from differential fluorescence line narrowing by Pieper and co-workers[38] on class IIa WSCP reconstituted with either *Chl a* or *Chl b* from cauliflower (*Brassica oleracea var. botrytis*). We then perform QM/MM as well as classical MD simulations to explore the ground-state potential energy surface of the system and later process the trajectory with ZINDO excited-state calculations based on the QM/MMpol approach we have recently developed,[36,37] which accounts for mutual pigment-protein polarization effects in a self-consistent way, in order to extract the corresponding spectral densities of *Chl a* and *Chl b* in the complex.

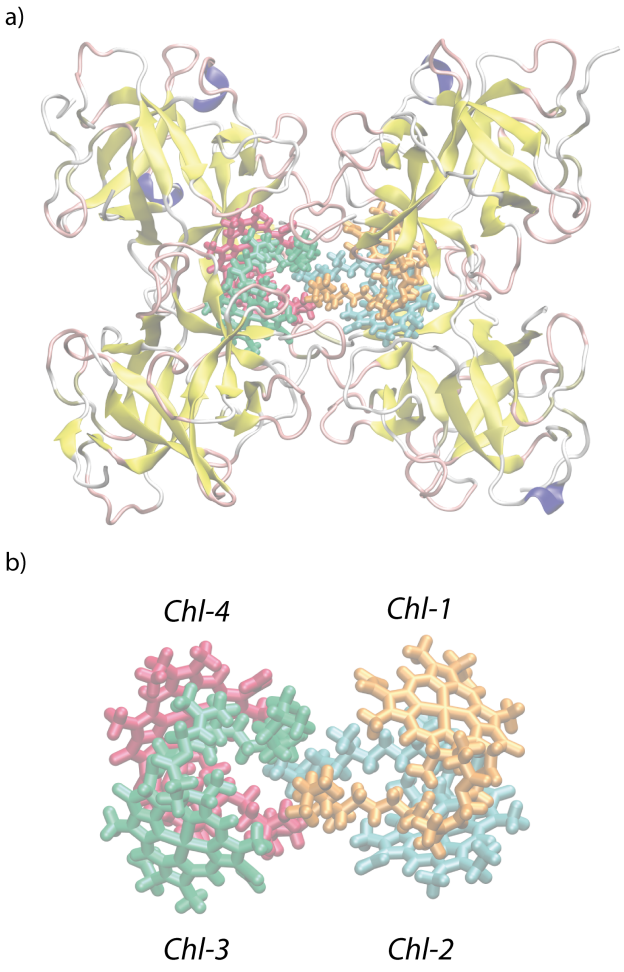

Figure 1. a) Structure of the water-soluble chlorophyll-binding protein. b) Detailed view of the four chlorophyll pigments.

The paper is organized in the following way. First, the methods and computational details – the extraction of the spectral density from the autocorrelation function and the details of the MD and the QM/MMpol excited-state calculations – are presented. Next, the results for both

WSCP with *Chl a* and WSCP with *Chl b* are shown and discussed. Finally, we provide the conclusions of our study and some perspectives on future developments for quantitative predictions of pigment-protein coupling in photosynthetic complexes.

2. Methods

2.1 Spectral densities

The spectral density, $J(\omega)$, describes the frequency-dependent coupling strength among electronic transitions and matrix vibrations, including both intramolecular pigment and intermolecular environmental modes. For practical purposes, it is often decomposed into two contributions:

$$J(\omega) = J_0(\omega) + J_{vib}(\omega) \quad (1)$$

where $J_0(\omega)$ describes the coupling of the pigments' excitations to a continuum of low-frequency damping modes due to the solvent and the protein environment, and $J_{vib}(\omega)$ accounts for the coupling with high-frequency modes, mostly coming from intramolecular pigment vibrations. The spectral density defines the total reorganization energy

$$\lambda = \int_0^\infty \frac{J(\omega)}{\omega} d\omega \quad (2)$$

The complete spectral density $J(\omega)$ can be estimated by simulating the time evolution of the electronic transition energies (site energies) of the pigments, although it is difficult to capture very low frequency modes in $J_0(\omega)$ because of the limited times currently affordable for such simulations. This strategy combines ground-state MD simulations and QM/MM excite-state calculations performed along the trajectory. Then, the spectral density of a given pigment *i* can be derived from the Fourier transform of the autocorrelation function of site energy fluctuations:[19,22,24]

$$J_i(\omega) = \frac{\beta\omega}{\pi} \int_0^\infty C_i^{cl}(t) cos(\omega t) dt \quad (3)$$

where $\beta = 1/(k_B T)$ and $C_i^{cl}(t)$ is the classical autocorrelation function of fluctuations in the site energy of pigment *i*:

$$C_i^{cl}(t_j) = \frac{1}{N-j}\sum_{k=1}^{N-j} \Delta E_i(t_j + t_k)\Delta E_i(t_k) \quad (4)$$

The expression in Eq. 3 has a classical pre-factor introduced to negate the temperature dependence of the classical correlation function, thus ensuring a temperature-independent spectral density.[24]

In the following sections, we describe the classical and PM6 QM/MM MD simulations as well as the ZINDO QM/MMpol excite-state calculations used to estimate the spectral densities of the chlorophylls in WSCP. In all cases, snapshots were extracted from the trajectories every 5 fs, yielding 20,000 frames that correspond to a total MD time of 100 ps. For each structure, QM/MMpol excited state calculations were performed either for all four chlorophylls (classical MD) or for *Chl a*-1 and *Chl a*-2 (*Chl b*-1 and *Chl b*-2), the two chlorophylls described at the QM level (QM/MM MD). The autocorrelation function for each pigment was calculated using Eq. 4 from the transition energy fluctuations computed every 5 fs, in order to capture the fastest oscillations, which have a period of ~20 fs. The autocorrelations were observed to decay within 4 ps, so autocorrelation functions of 4 ps length were computed using the 100 ps window by shifting its initial time by 1 ps. These then were averaged to give the final function for a given pigment. To minimize the effects of the noise in the spectral densities, the final autocorrelations were multiplied by a Gaussian envelope of variance $\sigma^2 = 3.6 \times 10^5$ fs^2 to ensure they converge to zero.[24] The high-frequency offset in the spectral densities was corrected with negligible effects in the low-frequency part by shifting the Fourier transform before its multiplication by the pre-factor.[28,29]

Here our theoretical estimates are compared to the experimental differential fluorescence line-narrowing (ΔFLN) data measured by Pieper and co-workers.[38,39] In these experiments, both the continuous $J_0(\omega)$ and the discrete $J_{vib}(\omega)$ components of the spectral density were estimated. In order to model $J_0(\omega)$, however, the log-normal expression and the corresponding parameters introduced by Kell and co-workers to describe the *Chl a* and *Chl b* WSCP ΔFLN spectra (parameters reported in Table 1 of Ref. [40]) are used; such an approach has been shown to describe better the phonon spectral density of different photosynthetic complexes compared to other expressions commonly used. On the other hand, the discrete $J_{vib}(\omega)$ component is modelled as a collection of damped quantum harmonic oscillators using the vibrational frequencies and

Huang-Rhys factors derived from the ΔFLN spectra (reported in Table 1 of Ref. 38). The complete experimental spectral densities were thus modelled using the following expressions:

$$J^{exp}(\omega) = J_0^{exp}(\omega) + J_{vib}^{exp}(\omega) \quad (5)$$

$$J_0^{exp}(\omega) = \sum_i \frac{\omega S_i}{\sigma_i\sqrt{2\pi}} e^{-[ln(\omega/\omega_i)]^2/2\sigma_i^2} \quad (6)$$

$$J_{vib}^{exp}(\omega) = \sum_q \frac{2\lambda_q}{\pi} \frac{\nu_q \omega_q^2 \omega}{\left(\omega_q^2-\omega^2\right)^2+\nu_q^2\omega^2} \quad (7)$$

where ω_i is the cutoff frequency, σ_i the standard deviation, and S_i the Huang-Rhys factor for the phonon contribution *i*. The discrete oscillators have frequencies ω_q with associated damping υ_q and reorganization energy $\lambda_q = s_q\omega_q$. The associated damping υ_q was set to 16.5 cm^{-1} in order to reproduce the overall Huang-Rhys factors 0.80 and 0.74 measured for the vibrational profile when Eq. 2 is applied to the set of discrete vibrations of *Chl a* and *Chl b* WSCP, respectively [38].

2.2 Molecular dynamics simulations

The *Chl a* and *Chl b* WSCP simulation systems were based on the X-ray crystal structure of class IIb WSCP homotretramer reported at 2.0 Å resolution by Horigome *et al*. (PDB code 2DRE).[41] The four chlorophylls in the asymmetric binding sites of the crystal were assigned as *Chl a* molecules (*Chl a* WSCP), so for the *Chl b* simulations we substituted those with four *Chl b* molecules. The missing residues in the PDB file were carefully added by selecting appropriate rotamers for the side chain groups in order to avoid any steric clash with the neighboring amino acids. The structure is organized as a dimer of dimers, despite the sequence identity of the four subunits. Protonation states of all residues were determined by computing their corresponding pKa's at neutral pH using the PROPKA3 server,[49,50] indicating a standard protonation state for all residues. The system was solvated in a TIP3P water box (a truncated octahedron with a buffer zone of 12 Å) using the Leap module of the Amber 12 suite of programs.[51] The protein was described using the parm99SB Amber force field.[52] In the classical MD simulations, *Chl a* was described using the parameters developed by Zhang and co-workers[53] based on a previous parameterization of bacteriochlorophyll performed by Ceccarelli *et al*.,[54] with slight modifications. First, in Zhang's force field the four nitrogen atom types correspond to one *ns* and

three *nmh*. In order to prevent a distortion of the in-plane position of the Mg atom occurring due to the *nmh-mgc-nmh* and *nmh-mgc-ns* angle bendings, a new nitrogen atom type was introduced (note that originally such bending angles had an equilibrium value of 90º, inappropriate when the two nitrogens involved are in opposite sides of the Mg atom, where this value should rather be 180º). Second, a few missing dihedral terms for *Chl a* were added, and new atom types and parameters needed to describe *Chl b* were assigned based on the general Amber force field (gaff).[55] Finally, the RESP charges for both *Chls* were estimated via the usual Amber RESP approach at the HF/6-31G(d) level using a geometry optimized at the B3LYP/6-311G(d,p) level of theory. The final system, which contained ~90,000 atoms, first underwent 50 ns of MD simulation at constant pressure (1 atm) and temperature (298 K) using standard coupling schemes using the Amber12 code.[51] SHAKE was used to restrain all bonds involving hydrogen, an integration time step of 1 fs, periodic boundary conditions, the Particle Mesh Ewald approach to account for long-range electrostatics, and a non-bonded cutoff equal to 8 Å. Afterwards, the trajectory was extended for 100 ps, and the coordinates were extracted every 5 fs in order to obtain the 20,000 structures used in the subsequent QM/MMpol calculations. Since the fastest oscillations in the chlorophyll transition energies have a period of about 20 fs, 5 fs is a reasonable choice for the estimation of their fluctuations both in terms of accuracy and computational cost, as shown in previous studies.[29,31]

For the *Chl a*-WSCP and *Chl b*-WSCP systems, 100 ps QM/MM MD simulations were run using the built-in semi-empirical QM/MM code available in Amber 12.[35] These runs were started from the same point as the 100 ps classical trajectory, *i.e.,* after 50 ns of classical MD simulation. The same conditions as for the classical MD were used, except the fact that *Chl*-1 and *Chl*-2 were described at the semi-empirical PM6 QM level of theory,[56] whereas *Chl*-3 and *Chl*-4 molecules were described through the classical force field to make the simulations feasible. Dispersion and hydrogen bond corrections with PM6 were not implemented because there were no available parameters for Mg. Finally, a QM-MM cutoff (*qmcut*) of 8 Å was utilized. In simulations that use periodic boundary conditions, the QM/MM cutoff only applies to the division of interactions between "direct" and "reciprocal" parts, and 8 Å is the recommended value.[51] As for the classical trajectory, 20,000 structures were extracted every 5 fs for the excited-state QM/MMpol calculations.

2.3 Polarizable QM/MM calculations

Excited state calculations along the structures extracted from the MD simulations were performed using the polarizable QM/MM strategy developed to study excited states and energy transfer in heterogeneous environments.[36,37,57] In particular, excited state calculations were performed for each chlorophyll, and the corresponding electronic couplings were calculated between the lowest-energy $\pi \rightarrow \pi^*$ Q_y states of the chlorophylls at the ZINDO level of theory.[58] For structures extracted from the QM/MM MD simulation, the excited state properties of *Chl*-1 and *Chl*-2 were computed, but no electronic couplings were estimated because the other chlorophylls were treated classically. The QM/MMpol model employed here couples a polarizable classical description of the protein and solvent environment based on the induced dipole model with a QM description of the pigments excited states. This requires assignment of atomic charges and polarizabilities to all MM atoms, and mutual polarization effects among the QM and MM regions are solved during the self-consistent-field process and the excited-state environment response. A detailed description of the methodology can be found in previous publications.[36,57]

Electronic couplings between the Q_y states also were computed using the structures extracted from the classical MD trajectory. In particular, the couplings are estimated from the transition densities derived from the ZINDO QM/MMpol excited state calculations, using the following expression:[36,37]

$$V = V_{coul} + V_{env} \tag{8}$$

$$V_{coul} = \int d\,\boldsymbol{r} \int d\boldsymbol{r}' \rho_A^{T*}(\boldsymbol{r}') \frac{1}{|\boldsymbol{r}'-\boldsymbol{r}|} \rho_D^T(\boldsymbol{r}) \tag{9}$$

$$V_{env} = -\sum_k \boldsymbol{\mu}_k^{ind} (\rho_D^T) \int d\boldsymbol{r} \frac{\rho_A^T(\boldsymbol{r})(\boldsymbol{r_k}-\boldsymbol{r})}{|\boldsymbol{r_k}-\boldsymbol{r}|^3} \tag{10}$$

where $\rho_{D/A}^T$ indicates the transition densities of the interacting pigments, and $\boldsymbol{\mu}_k^{ind}$ the induced dipoles describing the MM polarization response of the environment to a given transition density. The V_{coul} term describes the Coulomb interaction between the transition densities, thus representing an extension of the Förster dipole-dipole term that accounts for the shape of the

interacting molecules. The V_{env} term describes the environment-mediated contribution, which typically counteracts the V_{coul} term and therefore leads to an overall screening of the coupling. We can thus define an effective screening factor *s* as:[37]

$$s = \frac{(V_{coul}+V_{env})}{V_{coul}} \quad (11)$$

In all QM/MMpol calculations the AL parameters of the recent Amber pol12 polarizable force field to describe the protein MM region were adopted. For the water solvent, the POL3 model charges were used.[59] To speed up the calculations, the water molecular polarizability (1.44 Å^3) located on its center of mass was used instead of a three-point distributed polarizability model. Finally, in the QM/MMpol calculations the chlorophyll molecules not present in the QM region were described using the AL parameters from the Amber pol12 force field. In this case, a set of atomic charges either for *Chl a* or for *Chl b* consistent with the atomic polarizabilities were derived using the Polchat tool[60] by fitting to the electrostatic potential of the molecules, which were calculated at the MP2/aug-cc-pVTZ level of theory based on a B3LYP/6-311G(d,p) optimized geometry.

In the individual chlorophyll excited state calculations, the other three chlorophylls were described at the classical level, and similarly in the calculation of the electronic couplings, the two chlorophylls not involved in the interaction were also described classically. Water molecules were only included within 35 Å of the pigment(s) in the QM region, and atomic polarizabilties of MM atoms beyond 15 Å of the corresponding QM pigment(s) were set to zero. All QM/MMpol calculations were performed using a locally modified version of the Gaussian 09 code.[61]

3. Results and Discussion

3.1 Spectral densities of electron-vibrational coupling

In Figures 2 and 3 we report the spectral densities derived from QM/MM calculations performed over a classical or QM/MM MD trajectory for the WSCP complex reconstituted with either four *Chl a* or four *Chl b* molecules. These estimates are averaged over all chlorophylls in the complex (only *Chls* 1 and 2 when these are derived from the QM/MM MD simulations). In Figures S1 and S2 of the Supporting Information, we provide the spectral densities

corresponding to every chlorophyll in the complex, which are very similar to the averaged curve in all cases. This is a manifestation of the anticipated similar environment surrounding each pigment. In addition, this finding suggests that the 100 ps window of the MD trajectory suffices to converge the primary characteristics of the spectral densities, except for very low-frequency modes, which arise from slow protein motions characterized by longer timescales, which would require longer simulations to resolve these features.

In Figures 2 and 3, our predictions are plotted along with the spectral density measured by Pieper and co-workers from differential fluorescence line-narrowing spectra (ΔFLN) at 4.5 K for class IIa WSCP from cauliflower.[38–40] Compared to previous reports of simulated spectral densities, the availability of ΔFLN data reporting the coupling strength of all vibrations in the frequency ranges of interest, *i.e.,* from the environmental low-frequency region up to high-frequency intramolecular chlorophyll modes, allows us to critically assess the capability of the combined QM/MD strategy to describe the spectral density of this pigment-protein complex. Indeed, for *Chl a* the theoretical spectral density spans nearly the same range observed in the experiments, where the last peak appears at ~1650 cm^{-1}. However, for *Chl b* the simulated spectral density predicts two peaks at ~1730 cm^{-1} and ~1870 cm^{-1} at frequencies somewhat larger than 1681 cm^{-1}, the highest-frequency peak observed in experiments. As discovered by other groups, simulations dramatically overestimate the coupling to high frequency intramolecular motions at ~1600 cm^{-1}. This problem, previously found in other pigment-protein complexes, has been largely attributed to the classical nature of the MD trajectory used, which neglects quantum features of such high frequency motions.[17] As shown by Jing et al.[26] the displaced equilibrium geometry of the pigments described by the classical force field compared to the corresponding QM one consistent with the excited state calculations leads to an overestimation of the coupling strength. The classical force field, however, can also misrepresent the distribution of vibrational modes, *i.e.* the position of the peaks, due to the simplicity of the force field energy function. Indeed, the rich structure of peaks observed in the 1000-1600 cm^{-1} range from ΔFLN spectra is lost in the simulated spectral densities, or at most strongly underestimated, with the exception of the exaggerated peak at ~1600 cm^{-1} and the accurate peaks near ~1550-1600 cm^{-1}. The underestimation of the spectral density in the 1000-1600 cm^{-1} range thus seems to arise from an incorrect description of the position of the high-frequency vibrations, which incorrectly

accumulate near ~1600 cm^{-1} in contrast to experimental observation, rather than due to an incorrect description of the coupling strength due the geometry mismatch problem. This effect is clearly observed in the total accumulated reorganization energies shown in Figure 4, which abruptly increase near ~1600 cm^{-1}.

In sharp contrast, the simulated spectral densities at frequencies below 1000 cm^{-1} reproduce the experimental curve surprisingly well, with the notable exception of the exaggerated peak at ~280 cm^{-1} predicted in the *Chl a* WSCP complex, and the peak at ~660 cm^{-1} in the *Chl b* complex. For example, the agreement both in terms of peak position and of coupling strength for the main peaks around 550 cm^{-1} and 750 cm^{-1} is unexpected in light of previous reports of simulated spectral densities. Based on previous studies, we believe that the improved agreement at frequencies below 1000 cm^{-1} could either arise because we adopt an improved description of the vibrations in the classical force field in order to describe the pigments or because our excited state calculations explicitly account for environment polarization effects. Thus, the middle and low-frequency motions of the chlorophylls seem to be quite accurately described by the classical simulations coupled to the QM/MM semi-empirical estimation of the excited states, though the modes beyond 1000 cm^{-1} are poorly described.

The adoption of QM/MM MD simulations immensely improves the spectral density in the high-frequency region (750-1500 cm^{-1}), as shown in Figure 3. For the *Chl a* WSCP complex, all major experimental peaks in this range are observed with a corresponding peak in our simulations, although the intensity of some peaks is strongly overestimated, most notably at ~800 cm^{-1}, ~840 cm^{-1}, ~920 cm^{-1}, and ~990 cm^{-1}. In contrast to the simple force field energy function, thus, the PM6 QM/MM method seems to recover the proper distribution of pigment intramolecular vibrations in this frequency range suggested by experiments. There is a high degree of matching in terms of both frequency and intensity for ~1150 -1500 cm^{-1}. Nevertheless, some high-frequency peaks are still inaccurate. In particular, the feature at ~1550 cm^{-1} overestimates the electron-vibrational coupling, and the strong peak at ~1750 cm^{-1} is not observed by experiment. In sharp contrast, the description of the low and mid-frequency regions (50-750 cm^{-1}) degrades considerably compared to the results derived from the classical MD simulation. In this case, the QM/MM MD simulations lead to an overestimation of the spectral density at low frequencies,

especially in the case of *Chl a* WSCP. This problem suggests an underlying geometry mismatch problem in this strategy due to the use of the PM6 Hamiltonian to generate the QM/MM trajectories and the use of a different method, the ZINDO method, in the excited-state calculations. Because this overestimation mainly occurs in the low-frequency range, where intermolecular pigment-protein interactions can considerably impact the spectral density, we rather think that the overestimation arises due an additional problem, the misrepresentation of pigment-protein interactions along the QM/MM MD trajectory. Such misrepresentation is not unexpected, and it arises from an unbalanced description of the QM/MM boundary, since the QM/MM boundary adopts classical dispersion and repulsion Lennard-Jones parameters developed in the context of the Amber classical force field. Thus, they are balanced with a point-charge description of electrostatics to properly describe intermolecular interactions. However, in the QM/MM boundary, electrostatics are described as the interaction between the point charges of the MM region and the QM nuclei and electrons, so the Lennard-Jones parameters should be recalibrated in order to correct for this change in the treatment of electrostatics.

For the *Chl b* WSCP complex, the adoption of QM/MM MD simulations leads to an astonishing agreement between theory and experiment, in this case over the whole low, middle and high frequency ranges, with the only exception of the peak appearing at about ~1800 cm^{-1}, missing in the experimental curve, and also a non-negligible overestimation of the low-frequency features arising from the unbalanced treatment of the QM/MM boundary, as discussed previously. For example, the major peaks in the experimental curve at ~1300 cm^{-1}, ~1400 cm^{-1}, and ~1550 cm^{-1} are in excellent agreement with our simulations both in terms of frequency and electron-vibrational coupling. This is very encouraging, especially considering the use of semi-empirical QM methods both for the MD simulation and the excited-state calculations, which gives room for considerable improvements. Indeed, the PM6 method still suffers from important errors associated to the description of equilibrium geometries, dipole moments and noncovalent interactions,[62] and all of these errors can introduce important noise in our predictions. Unfortunately, improvements in this direction, like the introduction of explicit hydrogen-bond and dispersion corrections in PM6,[62] could not be adopted in this study due to the lack of parameters for Mg. The limitations of the PM6 method probably originate the exaggerated peaks predicted at ~1750-1800 cm^{-1} both for the *Chl a* and *Chl b* WSCP complexes in the QM/MM

MD results. Overall, we think that the adoption of more accurate density functional theory (DFT) methods in the QM/MM MD simulation, given that linear-scaling codes able to tackle large systems are becoming increasingly common, and the recalibration of the Lennard-Jones force field parameters for the description of the QM/MM boundary are expected to lead to a better quantitative accuracy in predicted spectral densities.

It is also worth recalling that the experimental spectral density was determined at 4.5 K for class IIa WSCP complexes, whereas our simulations are performed on class IIb WSCP at room temperature. Moreover, the QM/MM MD simulations adopted in this study are still classical in nature, but the forces are integrated over a QM/MM potential energy surface in order to describe the nuclear motions. Therefore, the improved QM/MM MD results suggest that the main problem in the popular QM/MD strategy is related to the geometry mismatch among the structures extracted from the MD trajectory and later used for QM excited states calculations, not to the quantum features of high-frequency vibrations, as these are not captured either by the classical or QM/MM simulations presented here.

Finally, we note that recent studies remark the key role that vibrations commensurating the energy difference among exciton states have in energy transfer dynamics and quantum coherence effects observed in photosynthetic complexes.[1413] In Figure 5 we provide a detailed comparison of the spectral densities predicted in this study in the 0-200 cm^{-1} range, not clearly visible in the previous figures, given that exciton states often have energetic differences in this energy region. The overall intensity of the spectral density in this range is comparable to experiment in the classical simulations, but it is exaggerated in the QM/MM results, an effect clearly seen in the total accumulated reorganization energies shown in Figure 4. As previously discussed, this overestimation most probably arises from inaccuracies related to the description of the QM/MM boundary in the QM/MM MD simulations. In the classical simulations, however, the spectral features in this energy range still do not accurately match the experiments. This is not unexpected given the limited 4 ps simulation times used to compute the autocorrelation functions in the derivation of the spectral density. Clearly, much longer simulation times would be needed to resolve the very low frequency features (<100 cm^{-1}).

The quality of the overall predicted spectral densities can be judged by inspection of Figure 4, in which we provide an estimate of the total accumulated reorganization energies as a function of the vibrational frequency range used for the integration. In the theoretical estimates based on classical MD trajectories, the agreement with experiment is excellent up to ~1000 cm^{-1}, illustrating the fact that the pigment-protein coupling is described better than in QM/MM simulations, probably due to the inaccuracies in the QM/MM boundary parameters previously discussed. After ~1000 cm^{-1}, however, the slope of the curve is better when the QM/MM MD trajectories are adopted, whereas the classical MD curves show a flat trend until ~1600 cm^{-1}, when the strongly exaggerated peak observed in the spectral densities gives a step-like increase in the reorganization energy not observed in the experimental counterpart. As we argue previously, this suggests that the classical force field is unable to describe the smooth distribution of vibrations in the 1000-1600 cm^{-1} observed experimentally and in the QM/MM MD results.

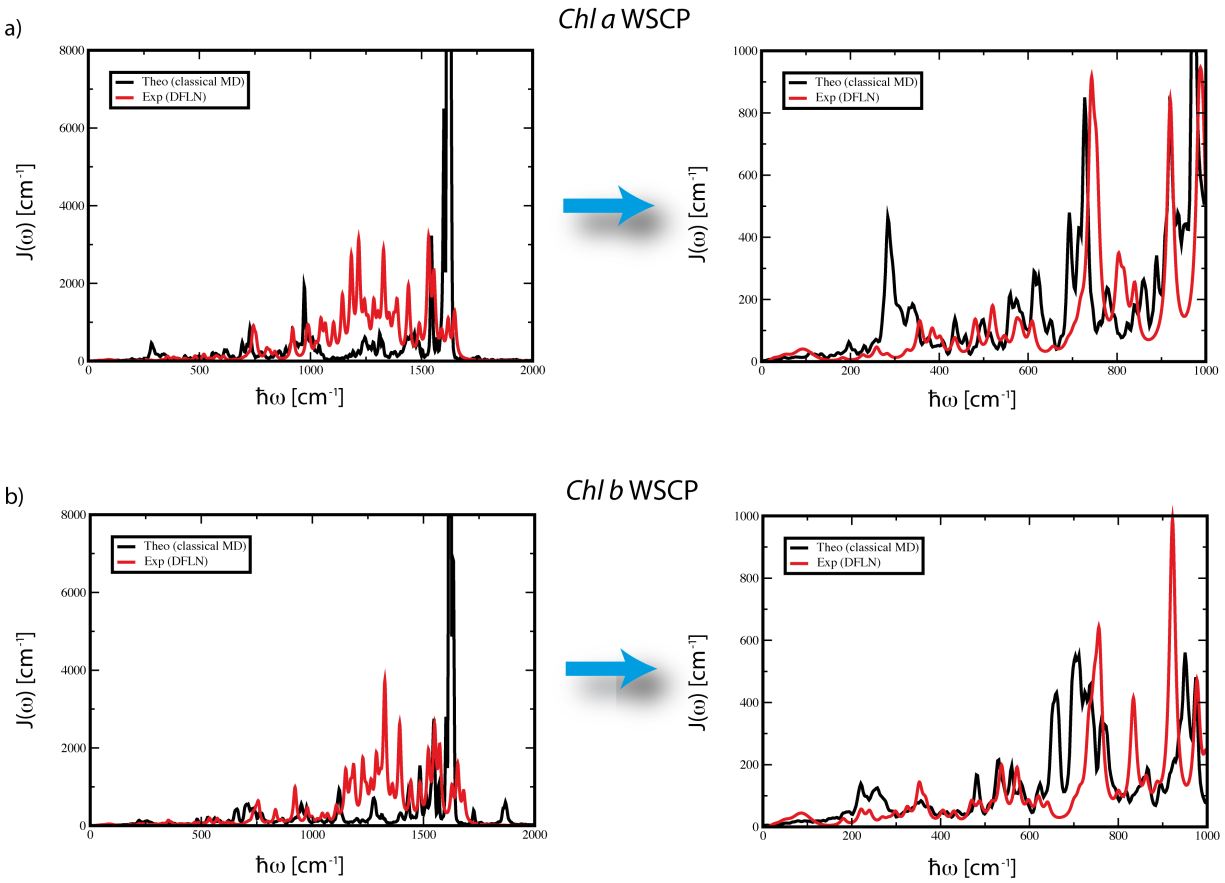

Figure 2. Spectral densities estimated from QM/MMpol excited state calculations performed along classical MD simulations compared to experimental ΔFLN data.[38–40]. a) *Chl a* WSCP; b) *Chl b* WSCP.

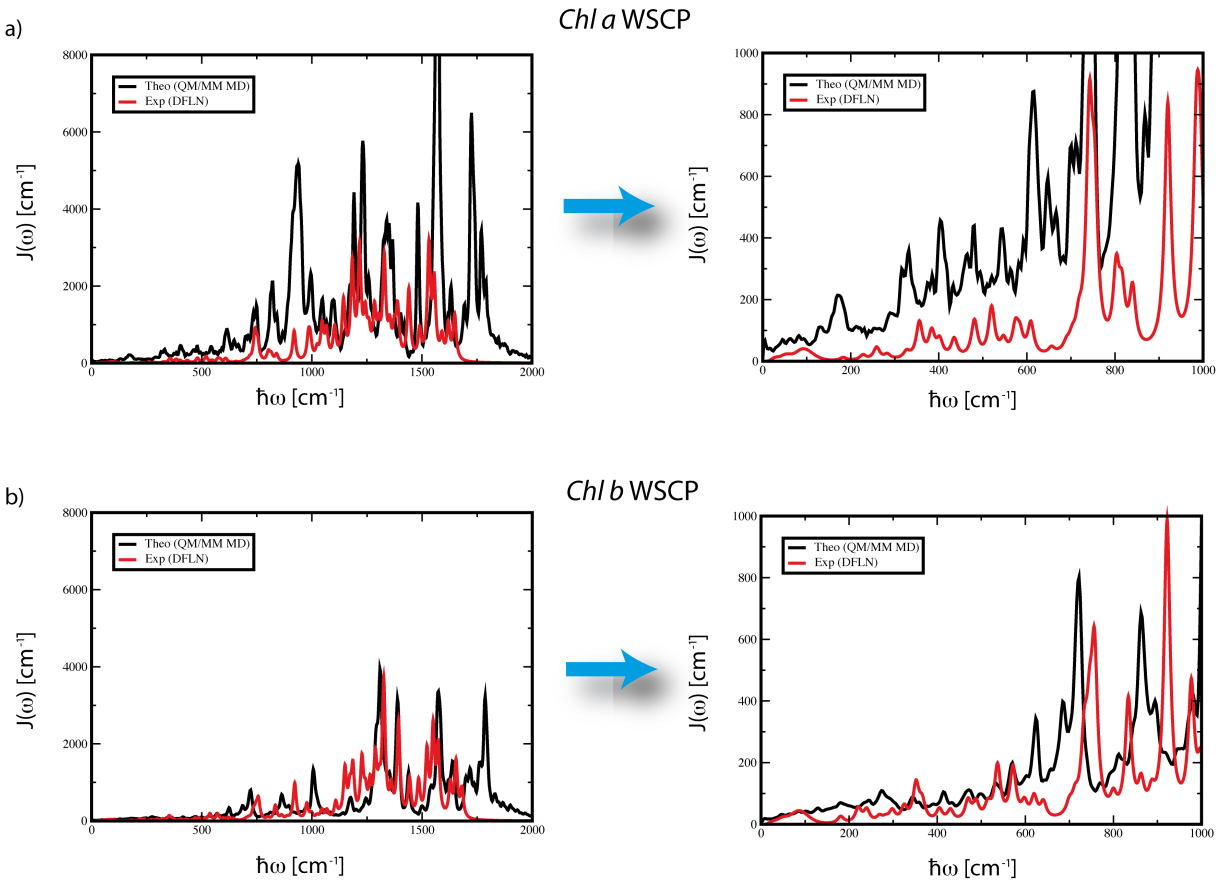

Figure 3. Spectral densities estimated from QM/MMpol excited state calculations performed along QM/MM MD simulations compared to experimental ΔFLN data.[38–40]. a) *Chl a* WSCP; b) *Chl b* WSCP.

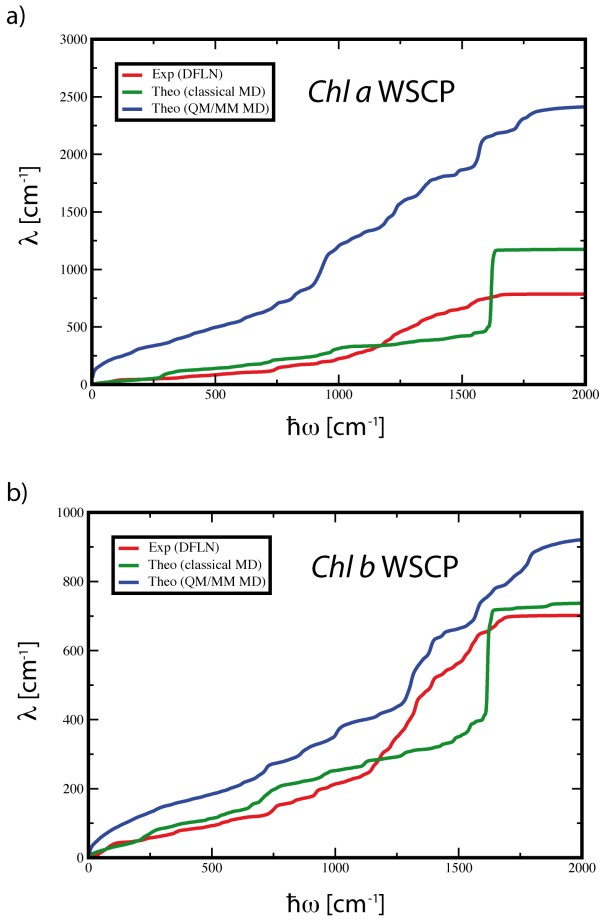

Figure 4. Total accumulated reorganization energy integrated from the spectral densities estimated from classical and QM/MM MD simulations compared to experimental ΔFLN data.[38–40]. a) *Chl a* WSCP; b) *Chl b* WSCP.

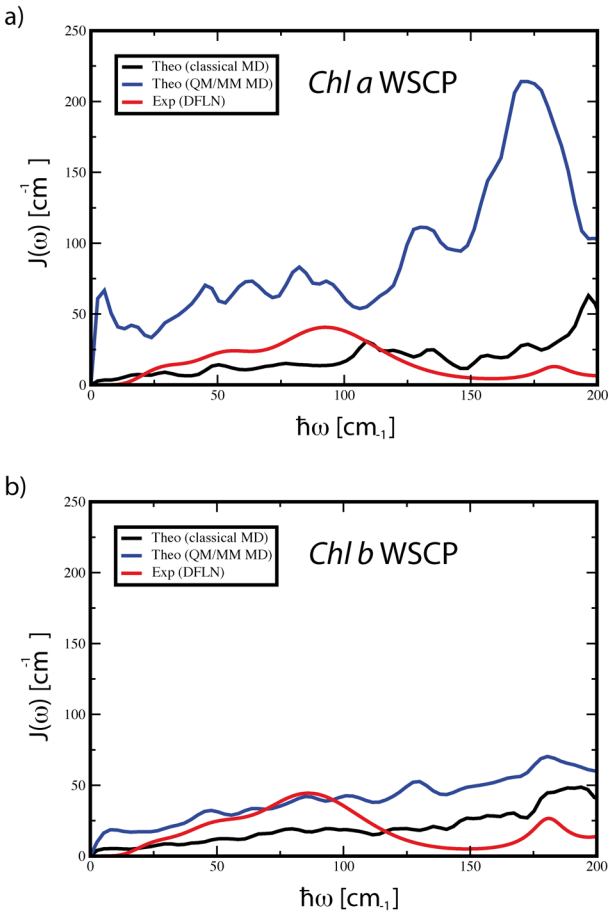

Figure 5. Detailed view of the spectral densities estimated from QM/MMpol excited state calculations performed along classical and QM/MM MD simulations in the low-frequency range and compared to experimental ΔFLN data.[38–40]. a) *Chl a* WSCP; b) *Chl b* WSCP.

3.2 Excitonic parameters

The relative simplicity of WSCP compared to other pigment-protein complexes makes it a logical system for benchmark studies for the improvement of energy transfer and spectral modeling theories. Multiple groups have contributed with different studies on WSCP.[38,39,42–48] In particular, Pieper and co-workers have provided an estimate of the electronic coupling between the *Chl*-1 and *Chl*-2 pigments both for class IIa WSCP complexes reconstituted with *Chl a* and *Chl b* from spectral hole-burning experiments.[39] In particular, by assuming that both Chls have

the same site energies, they derived V_{12} coupling values of 100 cm^{-1} and 85 cm^{-1} for *Chl a* and *Chl b* WSCP based on the difference of satellite hole positions, which should equal the excitonic splitting $2V_{12}$. If the simulated V_{12} and V_{34} values shown in Table 1 are averaged, the splitting is 186 cm^{-1} and 150 cm^{-1} for the *Chl a* and *Chl b* systems, respectively, assuming that *Chl* pairs 1-2 and 3-4 are symmetric in the homotetramer structure of class IIb WSCP. These estimates, which account for the dielectric screening effects exerted by the protein environment, thus overestimate the experimental values by nearly a factor of 2. This discrepancy in part arises from the exaggeration of the transition dipole moment of the Q_y *Chl a* and *Chl b* transitions. As reported in Table 2, our ZINDO QM/MMpol calculations predict an average transition dipole of 8.8 and 7.4 Debye for *Chl a* and *Chl b*, much larger than the values 4.0 and 3.6 Debye derived from the analysis of experimental data performed by Knox and Spring assuming a Lorentz effective field factor.[63,64] We note here that this analysis assumes that dipole strengths among different environments only change due to effective field factors (*i.e.* that the dipole is nonpolarizable), but not due to different intrinsic dipole strengths of the chlorophylls in the different environments, which are assumed to be the same and referred to as "vacuum" dipole strengths in a somewhat misleading term. Thus, we can directly compare our predicted ZINDO dipole values, which include polarization effects due to the surrounding environment, with the "vacuum" values derived by Knox and Spring analysis. Correcting the couplings in order to reproduce the effective dipole strength from this analysis would lead to quite small coupling values of 38 cm^{-1} and 35 cm^{-1}. Without dielectric screening effects, these would become 64 cm^{-1} and 58 cm^{-1}, rather similar to the 77 cm^{-1} and 69 cm^{-1} estimated by Renger and co-workers using the same chlorophylls effective dipole strength.[47] Moreover, we note that in our simulations the average angle among dipole moments, 28.0º (27.0º Chla-1/ Chla -2, 29.0º Chla-3/ Chla-4) and 37.5º (33.6º Chla-1/ Chla-2, 41.3º Chla-3/ Chla-4), are in excellent agreement with those derived recently by Dinh and Renger (30º and 39º), where also an increase of ~9º was needed in order to describe the changes among *Chl a* and *Chl b* WSCP spectra.[48] This variation arises from changes in the orientation of the *Chl b* dipole moment with respect to that of *Chl a* . These changes are due to the differences in electronic structure of the pigments, not the changes in the Chl dimer "open sandwich" structure; indeed, the “open sandwich” structure, or an angled gap between chlorophylls in a dimer, is maintained at ~52-55º for both *Chl a* and *Chl b*.

There are a few different possibilities for the disagreement among the experimental and predicted coupling value. The first possibility involves potential inaccuracies in the analysis of Knox and Spring, mainly related to the approximations underlying the Lorentz effective field factor, which only accounts for changes in the dipole strength due to effective fields but cannot describe changes in the intrinsic chlorophyll transition dipole arising from changes in the ground and excited states wave functions due to the surrounding environment, as discussed previously. For example, our ZINDO calculations predict a ~25% increase of the transition dipole when passing from vacuum to the protein environment. In this regard, our calculations would require an effective dipole of 6.5 and 5.6 Debye for *Chl a* and *Chl b* in order to reproduce the experimental coupling estimates.

Another reason for the mismatch could be due to inaccuracies in the dielectric screening effects as described by the QM/MMpol method. Indeed, the factor of ~0.60 describes a strong attenuation of the interaction, suggesting an effective optical dielectric constant (the inverse of the screening factor) equal to 1.66 for the *Chl*-1/*Chl*-2 interaction in both *Chl a* and *Chl b* WSCP complexes. We note here that this screening factor is well converged, since a screening factor of ~0.60 can be obtained using a larger polarization cutoff of up to 30 Å. Interestingly, the heterogeneous polarizable nature of the environment is reflected in the screening effects experienced by other pigment pairs, in the range 0.3-0.5, which describe effective dielectric constants in the range 2-3, as found for other pigment-protein complexes.[37,65]

Lastly, another potential problem is the assumption of equal site energies in the experimental estimate derived from excitonic splittings.[39] If the best coupling estimates are taken as 38 cm^{-1} and 35 cm^{-1}, which include dielectric screening effects and are consistent with Knox analysis, an asymmetry of about ~150 cm^{-1} would be needed to reproduce the experimental excitonic splittings. Such asymmetry could arise due to different packing of the phytyl chains in the hydrophobic pocket.[41] Indeed, our simulations predict energy differences among *Chl*-1/*Chl*-2 or *Chl*-3/*Chl*-4 of ~100-150 cm^{-1}, as shown in Tables 2 and 3, corresponding to the results derived from classical or QM/MM MD simulations. These smaller values for the electronic coupling (38 cm^{-1} and 35 cm^{-1}), however, could possibly not explain the strong redistribution of oscillator strength toward the high-energy exciton state observed experimentally, so a robust estimate of

the potential asymmetry among site energies should be explored by accurate simulation of the spectral line shapes in future studies.

Table 1. Average electronic couplings (cm^{-1}) calculated for the *Chl a* and *Chl b* WSCP complexes from classical MD trajectories. Screening factors are reported as lower triangular elements.

Chl a WSCP	Chla-1	Chla-2	Chla-3	Chla-4
Chla-1	--	183	15	31
Chla-2	0.60	--	31	9
Chla-3	0.37	0.49	--	188
Chla-4	0.46	0.32	0.58	--
Chl b WSCP	Chlb-1	Chlb-2	Chlb-3	Chlb-4
Chlb-1	--	145	10	17
Chlb-2	0.62	--	17	1
Chlb-3	0.40	0.53	--	154
Chlb-4	0.50	--[a]	0.59	--

[a]Screening factor not reliable due to the numerical inaccuracies related to the associated small coupling value.

Table 2. Average site energies (cm^{-1}) and transition dipole moments (Debye) calculated for the *Chl a* and *Chl b* WSCP complexes from classical MD trajectories.

	ΔE	$\langle\mu_x\rangle$	$\langle\mu_y\rangle$	$\langle\mu_z\rangle$	$\lvert\langle\mu\rangle\rvert$
Chl a WSCP					
Chla-1	12334	4.545	-3.399	6.595	8.701
Chla-2	12361	6.969	-0.353	5.369	8.804
Chla-3	12373	-6.545	3.946	-4.418	8.827
Chla-4	12158	-5.772	0.295	-6.859	8.969
Chl b WSCP					
Chlb-1	12911	2.892	-6.151	-2.498	7.241
Chlb-2	13049	4.898	-5.485	1.197	7.451
Chlb-3	12920	-4.756	4.184	3.949	7.464
Chlb-4	13014	-5.763	4.592	-1.204	7.466

Table 3. Average site energies (cm^{-1}) and transition dipole moments (Debye) calculated for the *Chl a* and *Chl b* WSCP complexes from QM/MM MD trajectories.

	ΔE	$\langle\mu_x\rangle$	$\langle\mu_y\rangle$	$\langle\mu_z\rangle$	$\lvert\langle\mu\rangle\rvert$
Chl a WSCP					
Chla-1	15361	3.844	-4.035	4.706	7.294
Chla-2	15360	5.101	0.970	5.474	7.545
Chl b WSCP					
Chlb-1	15086	2.963	-3.743	-5.243	7.091
Chlb-2	14975	3.331	-5.748	3.432	7.477

Conclusion

In this work, we have presented an improved strategy based on the combination of semi-empirical QM/MM MD simulations with QM/MMpol excited state calculations to predict the spectral density of electron-vibrational coupling for a pigment-protein complex. This approach is applied to the prediction of spectral densities of class IIb water-soluble chlorophyll-binding protein (WSCP) reconstituted with either *Chl a* or *Chl b* pigments, and the results are critically assessed by comparison with detailed differential fluorescence line-narrowing data measured at 4.5 K, as well as to predictions based on the usual MD/QM strategy based on classical MD simulations. The results show that the adoption of QM/MM MD simulations leads to a striking improvement of the predicted spectral densities in the middle and high-frequency regions, where the classical MD simulation is unable to capture the experimental features arising from pigment intramolecular vibrations. This demonstrates that accounting for the quantum features of the high-frequency pigment vibrations, neglected both in our classical and QM/MM simulations, is not critical in order to capture the characteristics of the spectral density, given that in the QM/MM simulation the propagation of the nuclear positions is still performed at the classical level but over a QM/MM potential energy surface. Instead, the so-called "geometry mismatch" problem related to the use of low-quality geometries described by a classical force field in the subsequent QM calculations is the origin for the poor description of pigment intramolecular features in spectral densities derived from classical MD simulations. In the WSCP complex, the classical force field adopted in this study misrepresents the distribution of chlorophyll vibrational modes in the 1000-1600 cm^{-1} range, thus leading to a strong underestimation of the experimental features observed in this spectral region. Nevertheless, the simulations still show important inaccuracies in the description of low-frequency features by using QM/MM MD simulations, probably related to an unbalanced treatment of Lennard-Jones dispersion-repulsion and electrostatic pigment-protein interactions in the QM/MM boundary, and suggest that Lennard-Jones potentials should be re-parameterized in this case in order to be consistent with the QM/MM treatment of electrostatics in this boundary. Despite their shortcomings, these results are very encouraging, especially taking into account the relatively inaccurate semi-empirical level of theory used both for the QM/MM MD and the QM/MMpol excited state calculations. There is much room for improvement in such theoretical studies; for instance, adopting DFT methodologies could lead to even more accurate results.

Finally, we provide an estimate of the site energies and the electronic coupling strength corresponding to the chlorophyll pigments in WSCP. The results suggest that the polarizable environment of the protein is quite heterogeneous, leading to a substantial range of dielectric screening effects as experienced by the different chlorophylls in the complex, with effective dielectric constants in the 1.5-3 range. We also critically compare our results with the experimental estimate of the electronic coupling in the strongly coupled dimer provided by Pieper and co-workers from spectral hole-burning experiments performed in class IIa WSCP by assuming symmetric site energies.[39] The results indicate that effective dipoles equal to 6.5 Debye (*Chl a*) and 5.6 Debye (*Chl b*) in the WSCP complex are necessary in order to reproduce the experimentally observed excitonic splittings, assuming the sites indeed have equal site energies. Our simulations, however, suggest a slight asymmetry in the site energies of the *Chl*-1/*Chl*-2 and *Chl*-3/*Chl*-4 pigments on the order of ~100-150 cm^{-1}, which would then be compatible with effective dipoles equal to 4.0 and 3.6 Debye derived in previous studies and commonly assumed in the field. In future studies, the accurate value for such asymmetry in site energies should be investigated in detail by simulating the spectral line shapes of the complex.

Supporting Information Available

Figures of spectral densities and table of reorganization energies of the individual chlorophylls, MD-averaged pigment positions and interpigment separations, classical force field parameters for *Chl a* and *Chl b* used in the MD simulation and in QM/MMpol excited state calculations. This information is available free of charge via the Internet at http://pubs.acs.org.

Acknowledgements

We acknowledge computational resources provided by the Consorci de Serveis Universitaris de Catalunya. Financial support for A. R. was provided by a Fulbright Full Grant, a grant provided by the American and Spanish Fulbright Commissions. C. C. acknowledges support from the Ministerio de Economía y Competitividad (MINECO) of Spain (grants CTQ2012-36195 and RYC2011-08918) and the Agència de Gestió d'Ajuts Universitaris i de Recerca from Generalitat de Catalunya (GENCAT) (SGR2014-1189). Many thanks to Prof. Benedetta Menucci and her group for fruitful discussions on polarizable force fields, and to Prof. Thomas Renger for

valuable insights on the spectral densities derived from differential fluorescence line-narrowing spectra.

References

(1) Ishizaki, A.; Fleming, G. R. Quantum Coherence in Photosynthetic Light Harvesting. *Annu. Rev. Condens. Matter Phys.* **2012**, *3*, 333–361.

(2) Huelga, S. F.; Plenio, M. B. Vibrations, Quanta and Biology. *Contemp. Phys.* **2013**, *54*, 181–207.

(3) Chenu, A.; Scholes, G. D. Coherence in Energy Transfer and Photosynthesis. *Annu. Rev. Phys. Chem.* **2015**, *66*, 69–96.

(4) Scholes, G. D.; Fleming, G. R.; Olaya-Castro, A.; van Grondelle, R. Lessons from Nature about Solar Light Harvesting. *Nat. Chem.* **2011**, *3*, 763–774.

(5) Ball, P. The Dawn of Quantum Biology. *Nature* **2011**, *474*, 272–274.

(6) Engel, G. S.; Calhoun, T. R.; Read, E. L.; Ahn, T. K.; Mancal, T.; Cheng, Y. C.; Blankenship, R. E.; Fleming, G. R. Evidence for Wavelike Energy Transfer through Quantum Coherence in Photosynthetic Systems. *Nature* **2007**, *446*, 782–786.

(7) Lee, H.; Cheng, Y.-C.; Fleming, G. R. Coherence Dynamics in Photosynthesis: Protein Protection of Excitonic Coherence. *Science (80-.).* **2007**, *316*, 1462–1465.

(8) Collini, E.; Wong, C. Y.; Wilk, K. E.; Curmi, P. M. G.; Brumer, P.; Scholes, G. D. Coherently Wired Light-Harvesting in Photosynthetic Marine Algae at Ambient Temperature. *Nature* **2010**, *463*, 644–647.

(9) Ishizaki, A.; Calhoun, T. R.; Schlau-Cohen, G. S.; Fleming, G. R. Quantum Coherence and Its Interplay with Protein Environments in Photosynthetic Electronic Energy Transfer. *Phys. Chem. Chem. Phys.* **2010**, *12*, 7319–7337.

(10) Fassioli, F.; Dinshaw, R.; Arpin, P. C.; Scholes, G. D. Photosynthetic Light Harvesting: Excitons and Coherence. *J. R. Soc. Interface* **2013**, *11*, 20130901.

(11) Olbrich, C.; Strümpfer, J.; Schulten, K.; Kleinekathöfer, U. Quest for Spatially Correlated Fluctuations in the FMO Light-Harvesting Complex. *J. Phys. Chem. B* **2011**, *115*, 758–764.

(12) Viani, L.; Curutchet, C.; Mennucci, B. Spatial and Electronic Correlations in the PE545 Light-Harvesting Complex. *J. Phys. Chem. Lett.* **2013**, *4*, 372–377.

(13) O'Reilly, E. J.; Olaya-Castro, A.; O'Reilly, E. J.; Olaya-Castro, A. Non-Classicality of the Molecular Vibrations Assisting Exciton Energy Transfer at Room Temperature. *Nat. Commun.* **2014**, *5*, 3012.

(14) Chin, a. W.; Prior, J.; Rosenbach, R.; Caycedo-Soler, F.; Huelga, S. F.; Plenio, M. B. The Role of Non-Equilibrium Vibrational Structures in Electronic Coherence and Recoherence in Pigment–protein Complexes. *Nat. Phys.* **2013**, *9*, 113–118.

(15) Hayes, D.; Engel, G. S. Extracting the Excitonic Hamiltonian of the Fenna-Matthews-Olson Complex Using Three-Dimensional Third-Order Electronic Spectroscopy. *Biophys. J.* **2011**, *100*, 2043–2052.

(16) Renger, T.; Müh, F.; Muh, F. Understanding Photosynthetic Light-Harvesting: A Bottom up Theoretical Approach. *Phys. Chem. Chem. Phys.* **2013**, *15*, 3348–3371.

(17) Jurinovich, S.; Viani, L.; Curutchet, C.; Mennucci, B. Limits and Potentials of Quantum Chemical Methods in Modelling Photosynthetic Antennae. *Phys. Chem. Chem. Phys.* **2015**, DOI: 10.1039/C5CP00986C.

(18) Jankowiak, R.; Reppert, M.; Zazubovich, V.; Pieper, J.; Reinot, T. Site Selective and Single Complex Laser-Based Spectroscopies: A Window on Excited State Electronic Structure, Excitation Energy Transfer, and Electron–Phonon Coupling of Selected Photosynthetic Complexes. *Chem. Rev.* **2011**, *111*, 4546–4598.

(19) Damjanovic, A.; Kosztin, I.; Kleinekathofer, U.; Schulten, K.; Damjanović, A.; Kosztin, I.; Kleinekathöfer, U.; Schulten, K. Excitons in a Photosynthetic Light-Harvesting System: A Combined Molecular Dynamics, Quantum Chemistry, and Polaron Model Study. *Phys. Rev. E* **2002**, *65*, 31919.

(20) Janosi, L.; Kosztin, I.; Damjanovic, A.; Damjanović, A. Theoretical Prediction of Spectral and Optical Properties of Bacteriochlorophylls in Thermally Disordered LH2 Antenna Complexes. *J. Chem. Phys.* **2006**, *125*, 14903.

(21) Olbrich, C.; Kleinekathofer, U. Time-Dependent Atomistic View on the Electronic Relaxation in Light-Harvesting System II. *J. Phys. Chem. B* **2010**, *114*, 12427–12437.

(22) Olbrich, C.; Strumpfer, J.; Schulten, K.; Kleinekathofer, U. Theory and Simulation of the Environmental Effects on FMO Electronic Transitions. *J. Phys. Chem. Lett.* **2011**, *2*, 1771–1776.

(23) Shim, S.; Rebentrost, P.; Valleau, S.; Aspuru-Guzik, A. Atomistic Study of the Long-Lived Quantum Coherences in the Fenna-Matthews-Olson Complex. *Biophys. J.* **2012**, *102*, 649–660.

(24) Valleau, S. S.; Eisfeld, A.; Aspuru-Guzik, A. A. On the Alternatives for Bath Correlators and Spectral Densities from Mixed Quantum-Classical Simulations. *J. Chem. Phys.* **2012**, *137*, 224103.

(25) Renger, T.; Klinger, A.; Steinecker, F.; Schmidt am Busch, M.; Numata, J.; Müh, F. Normal Mode Analysis of the Spectral Density of the Fenna-Matthews-Olson Light-Harvesting Protein: How the Protein Dissipates the Excess Energy of Excitons. *J. Phys. Chem. B* **2012**, *116*, 14565–14580.

(26) Jing, Y. Y.; Zheng, R. H.; Li, H. X.; Shi, Q. Theoretical Study of the Electronic-Vibrational Coupling in the Q(y) States of the Photosynthetic Reaction Center in Purple Bacteria. *J. Phys. Chem. B* **2012**, *116*, 1164–1171.

(27) Kim, H. W.; Kelly, A.; Park, J. W.; Rhee, Y. M. All-Atom Semiclassical Dynamics Study of Quantum Coherence in Photosynthetic Fenna–Matthews–Olson Complex. *J. Am. Chem. Soc.* **2012**, *134*, 11640–11651.

(28) Aghtar, M.; Liebers, J.; Strumpfer, J.; Schulten, K.; Kleinekathöfer, U.; Strümpfer, J.; Schulten, K.; Kleinekathöfer, U. Juxtaposing Density Matrix and Classical Path-Based Wave Packet Dynamics. *J. Chem. Phys.* **2012**, *136*, 214101.

(29) Aghtar, M.; Strumpfer, J.; Olbrich, C.; Schulten, K.; Kleinekathöfer, U. The FMO Complex in a Glycerol–Water Mixture. *J. Phys. Chem. B* **2013**, *117*, 7157–7163.

(30) Rivera, E.; Montemayor, D.; Masia, M.; Coker, D. F. Influence of Site-Dependent Pigment-Protein Interactions on Excitation Energy Transfer in Photosynthetic Light Harvesting. *J. Phys. Chem. B* **2013**, *117*, 5510–5521.

(31) Viani, L.; Corbella, M.; Curutchet, C.; O'Reilly, E. J.; Olaya-Castro, A.; Mennucci, B. Molecular Basis of the Exciton-Phonon Interactions in the PE545 Light-Harvesting Complex. *Phys. Chem. Chem. Phys.* **2014**, *16*, 16302–16311.

(32) Aghtar, M.; Strumpfer, J.; Olbrich, C.; Schulten, K.; Kleinekathöfer, U. Different Types of Vibrations Interacting with Electronic Excitations in Phycoerythrin 545 and Fenna–Matthews–Olson Antenna Systems. *J. Phys. Chem. Lett.* **2014**, *5*, 3131–3137.

(33) Fujita, T.; Huh, J.; Saikin, S. K.; Brookes, J. C.; Aspuru-Guzik, A. Theoretical Characterization of Excitation Energy Transfer in Chlorosome Light-Harvesting Antennae from Green Sulfur Bacteria. *Photosynth. Res.* **2014**, *120*, 273–289.

(34) Huh, J.; Saikin, S. K.; Brookes, J. C.; Valleau, S.; Fujita, T.; Aspuru-Guzik, A. Atomistic Study of Energy Funneling in the Light-Harvesting Complex of Green Sulfur Bacteria. *J. Am. Chem. Soc.* **2014**, *136*, 2048–2057.

(35) Walker, R. C.; Crowley, M. F.; Case, D. A. The Implementation of a Fast and Accurate QM/MM Potential Method in Amber. *J. Comput. Chem.* **2008**, *29*, 1019–1031.

(36) Curutchet, C.; Munoz-Losa, A.; Monti, S.; Kongsted, J.; Scholes, G. D.; Mennucci, B. Electronic Energy Transfer in Condensed Phase Studied by a Polarizable QM/MM Model. *J. Chem. Theory Comput.* **2009**, *5*, 1838–1848.

(37) Curutchet, C.; Kongsted, J.; Muñoz-Losa, A.; Hossein-Nejad, H.; Scholes, G. D.; Mennucci, B. Photosynthetic Light-Harvesting Is Tuned by the Heterogeneous Polarizable Environment of the Protein. *J. Am. Chem. Soc.* **2011**, *133*, 3078–3084.

(38) Pieper, J.; Rätsep, M.; Trostmann, I.; Paulsen, H.; Renger, G.; Freiberg, A. Excitonic Energy Level Structure and Pigment-Protein Interactions in the Recombinant Water-Soluble Chlorophyll Protein. I. Difference Fluorescence Line-Narrowing. *J. Phys. Chem. B* **2011**, *115*, 4042–4052.

(39) Pieper, J.; Rätsep, M.; Trostmann, I.; Schmitt, F.-J.; Theiss, C.; Paulsen, H.; Eichler, H. J.; Freiberg, A.; Renger, G. Excitonic Energy Level Structure and Pigment-Protein Interactions in the Recombinant Water-Soluble Chlorophyll Protein. II. Spectral Hole-Burning Experiments. *J. Phys. Chem. B* **2011**, *115*, 4053–4065.

(40) Kell, A.; Feng, X.; Reppert, M.; Jankowiak, R. On the Shape of the Phonon Spectral Density in Photosynthetic Complexes. *J. Phys. Chem. B* **2013**, *117*, 7317–7323.

(41) Horigome, D.; Satoh, H.; Itoh, N.; Mitsunaga, K.; Oonishi, I.; Nakagawa, A.; Uchida, A. Structural Mechanism and Photoprotective Function of Water-Soluble Chlorophyll-Binding Protein. *J. Biol. Chem.* **2007**, *282*, 6525–6531.

(42) Hughes, J. L.; Razeghifard, R.; Logue, M.; Oakley, A.; Wydrzynski, T.; Krausz, E. Magneto-Optic Spectroscopy of a Protein Tetramer Binding Two Exciton-Coupled Chlorophylls. *J. Am. Chem. Soc.* **2006**, *128*, 3649–3658.

(43) Renger, T.; Trostmann, I.; Theiss, C.; Madjet, M. E.; Richter, M.; Paulsen, H.; Eichler, H. J.; Knorr, A.; Renger, G. Refinement of a Structural Model of a Pigment−Protein Complex by Accurate Optical Line Shape Theory and Experiments. *J. Phys. Chem. B* **2007**, *111*, 10487–10501.

(44) Theiss, C.; Trostmann, I.; Andree, S.; Schmitt, F. J.; Renger, T.; Eichler, H. J.; Paulsen, H.; Renger, G. Pigment - Pigment and Pigment - Protein Interactions in Recombinant Water-Soluble Chlorophyll Proteins (WSCP) from Cauliflower. *J. Phys. Chem. B* **2007**, *111*, 13325–13335.

(45) Renger, G.; Pieper, J.; Theiss, C.; Trostmann, I.; Paulsen, H.; Renger, T.; Eichler, H. J.; Schmitt, F. J. Water Soluble Chlorophyll Binding Protein of Higher Plants: A Most Suitable Model System for Basic Analyses of Pigment-Pigment and Pigment-Protein Interactions in Chlorophyll Protein Complexes. *J. Plant Physiol.* **2011**, *168*, 1462–1472.

(46) Alster, J.; Lokstein, H.; Dostál, J.; Uchida, A.; Zigmantas, D. 2D Spectroscopy Study of Water-Soluble Chlorophyll-Binding Protein from Lepidium Virginicum. *J. Phys. Chem. B* **2014**, *118*, 3524–3531.

(47) Renger, T.; Madjet, M. E.; Müh, F.; Trostmann, I.; Schmitt, F. J.; Theiss, C.; Paulsen, H.; Eichler, H. J.; Knorr, a.; Renger, G. Thermally Activated Superradiance and Intersystem Crossing in the Water-Soluble Chlorophyll Binding Protein. *J. Phys. Chem. B* **2009**, *113*, 9948–9957.

(48) Dinh, T.-C.; Renger, T. Towards an Exact Theory of Linear Absorbance and Circular Dichroism of Pigment-Protein Complexes: Importance of Non-Secular Contributions. *J. Chem. Phys.* **2015**, *142*, 034104.

(49) Olsson, M. H. M.; SØndergaard, C. R.; Rostkowski, M.; Jensen, J. H. PROPKA3: Consistent Treatment of Internal and Surface Residues in Empirical P K a Predictions. *J. Chem. Theory Comput.* **2011**, *7*, 525–537.

(50) Søndergaard, C. R.; Olsson, M. H. M.; Rostkowski, M.; Jensen, J. H. Improved Treatment of Ligands and Coupling Effects in Empirical Calculation and Rationalization of PKa Values. *J. Chem. Theory Comput.* **2011**, *7*, 2284–2295.

(51) Case, D. A.; Darden, T. A.; T.E. Cheatham, I.; Simmerling, C. L.; Wang, J.; Duke, R. E.; Luo, R.; Walker, R. C.; Zhang, W.; Merz, K. M.; Roberts, B.; Hayik, S.; Roitberg, A.; Seabra, G.; Swails, J.; Götz, A. W.; Kolossváry, I.; Wong, K. F.; Paesani, F.; Vanicek, J.; Wolf, R. M.; Liu, J.; Wu, X.; Brozell, S. R.; Steinbrecher, T.; Gohlke, H.; Cai, Q.; Ye, X.; Wang, J.; Hsieh, M.-J.; Cui, G.; Roe, D. R.; Mathews, D. H.; Seetin, M. G.; Salomon-Ferrer, R.; Sagui, C.; Babin, V.; Luchko, T.; Gusarov, S.; Kovalenko, A.; Kollman, P. A. AMBER 12. University of California: San Francisco, 2012.

(52) Hornak, V.; Abel, R.; Okur, A.; Strockbine, B.; Roitberg, A.; Simmerling, C. Comparison of Multiple Amber Force Fields and Development of Improved Protein Backbone Parameters. *Proteins-Structure Funct. Bioinforma.* **2006**, *65*, 712–725.

(53) Zhang, L.; Silva, D.-A.; Yan, Y.; Huang, X. Force Field Development for Cofactors in the Photosystem II. *J. Comput. Chem.* **2012**, *33*, 1969–1980.

(54) Ceccarelli, M.; Procacci, P.; Marchi, M. An Ab Initio Force Field for the Cofactors of Bacterial Photosynthesis. *J. Comput. Chem.* **2003**, *24*, 129–142.

(55) Wang, J. M.; Wolf, R. M.; Caldwell, J. W.; Kollman, P. A.; Case, D. A. Development and Testing of a General Amber Force Field. *J. Comput. Chem.* **2004**, *25*, 1157–1174.

(56) Stewart, J. J. P. Optimization of Parameters for Semiempirical Methods V: Modification of NDDO Approximations and Application to 70 Elements. *J. Mol. Model.* **2007**, *13*, 1173–1213.

(57) Curutchet, C.; Novoderezhkin, V. I.; Kongsted, J.; Muñoz-Losa, A.; Van Grondelle, R.; Scholes, G. D.; Mennucci, B. Energy Flow in the Cryptophyte PE545 Antenna Is Directed by Bilin Pigment Conformation. *J. Phys. Chem. B* **2013**, *117*, 4263–4273.

(58) Zerner, M. C. Semi Empirical Molecular Orbital Methods. In *Reviews of Computational Chemistry, Vol. 2*; Lipkowitz, K. B., Boyd, D. B., Eds.; VCH: New York, 1991; pp 313–366.

(59) Caldwell, J. W.; Kollman, P. A. Structure and Properties of Neat Liquids Using Nonadditive Molecular Dynamics: Water, Methanol, and N-Methylacetamide. *J. Phys. Chem.* **1995**, *99*, 6208–6219.

(60) Caprasecca, S.; Curutchet, C.; Mennucci, B.; Jurinovich, S. PolChat: A Polarisation-Consistent Charge Fitting Tool. Molecolab Tools, University of Pisa, 2014. Available at: http://www.dcci.unipi.it/molecolab. (Last accessed on 01/19/2015).

(61) Frisch, M. J.; Trucks, G. W.; Schlegel, H. B.; Scuseria, G. E.; Robb, M. A.; Cheeseman, J. R.; Scalmani, G.; Barone, V.; Mennucci, B.; Petersson, G. A.; Nakatsuji, H.; Caricato, M.; Li, X.; Hratchian, H. P.; Izmaylov, A. F.; Bloino, J.; Zheng, G.; Sonnenberg, J. L.; Hada, M.; Ehara, M.; Toyota, K.; Fukuda, R.; Hasegawa, J.; Ishida, M.; Nakajima, T.; Honda, Y.; Kitao, O.; Nakai, H.; Vreven, T.; Montgomery J. A., J.; Peralta, J. E.; Ogliaro, F.; Bearpark, M.; Heyd, J. J.; Brothers, E.; Kudin, K. N.; Staroverov, V. N.; Kobayashi, R.; Normand, J.; Raghavachari, K.; Rendell, A.; Burant, J. C.; Iyengar, S. S.; Tomasi, J.; Cossi, M.; Rega, N.; Millam, N. J.; Klene, M.; Knox, J. E.; Cross, J. B.; Bakken, V.; Adamo, C.; Jaramillo, J.; Gomperts, R.; Stratmann, R. E.; Yazyev, O.; Austin, A. J.; Cammi, R.; Pomelli, C.; Ochterski, J. W.; Martin, R. L.; Morokuma, K.; Zakrzewski, V. G.; Voth, G. A.; Salvador, P.; Dannenberg, J. J.; Dapprich, S.; Daniels, A. D.; Farkas, Ö.; Foresman, J. B.; Ortiz, J. V; Cioslowski, J.; Fox, D. J. Gaussian 09, Revision A.2. Gaussian, Inc.: Wallingford CT 2009.

(62) Korth, M.; Pitoňák, M.; Řezáč, J.; Hobza, P. A Transferable H-Bonding Correction for Semiempirical Quantum-Chemical Methods. *J. Chem. Theory Comput.* **2010**, *6*, 344–352.

(63) Knox, R. S. Dipole and Oscillator Strengths of Chromophores in Solution. *Photochem. Photobiol.* **2003**, *77*, 492–496.

(64) Knox, R. S.; Spring, B. Q. Dipole Strengths in the Chlorophylls. *Photochem. Photobiol.* **2003**, *77*, 497–501.

(65) Jurinovich, S.; Curutchet, C.; Mennucci, B. The Fenna-Matthews-Olson Protein Revisited: A Fully Polarizable (TD)DFT/MM Description. *ChemPhysChem* **2014**, *15*, 3194–3204.

TOC GRAPHIC

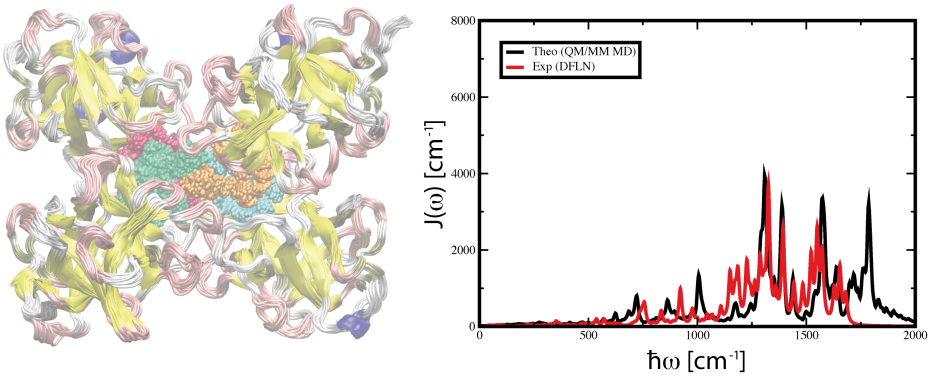
Theo (QM/MM MD)
Exp (DFLN)
J(ω) [cm-1]
ħω [cm-1]
0
2000
4000
6000
8000
500
1000
1500
2000